Applications in Energy and Combustion Science 5 (2021) 100019

Contents lists available at ScienceDirect

Applications in Energy and Combustion Science

journal homepage: www.elsevier.com/locate/jaecs

Towards system pressure scaling of gas assisted coaxial burner nozzles – An empirical model

Simon Wachter[a,*], Tobias Jakobs[a], Thomas Kolb[a,b]

[a] Institute for Technical Chemistry, Karlsruhe Institute of Technology, 76344 Eggenstein-Leopoldshafen, Germany
[b] Engler-Bunte-Institute, Karlsruhe Institute of Technology, 76131 Karlsruhe, Germany

ARTICLE INFO

Keywords:
Scaling
Nozzle
Pressure
Empirical model
Atomization

ABSTRACT

The present study investigates the influence of system pressure, gas velocity, and annular gas gap width on the resulting droplet size. Three external-mixing twin-fluid atomizers are operated at a constant liquid mass flow. The nozzle geometry is kept similar, except that the annular gas gap width is changed. At every system pressure level (1 – 21 bar), three different gas velocities were investigated by changing the gas mass flow. High-speed camera images are used for observation of primary breakup and discussed with regard to local measurements of droplet size performed by a phase Doppler anemometer. The gas momentum flux as well as the gas momentum flow were applied to describe the atomization process under varying operating conditions. Finally, an empirical model is derived, enabling the system pressure scaling of external-mixing twin-fluid atomizers for the range of gas momentum flow under investigation.

1. Introduction

Spray processes are often utilized in industrial production; however, the influence of process conditions on atomization is not yet fully understood. In particular, limited literature is available on twin-fluid atomization at increased system pressure that is commonly applied in high-pressure entrained flow gasifiers (EFGs). These large-scale energy conversion systems can play a key role in future resource and energy supply. In EFGs, highly viscous liquid or suspension fuels with complex flow behavior (e.g., non-Newtonian) are typically atomized at elevated system pressures (in the range of 40–80 bar) [1]. Oxygen and steam serve as atomization media to guarantee high-quality syngas. Using oxygen as a gasification agent and at the same time as atomization agent, leads to a coupling of process stoichiometry and nozzle operating conditions with respect to the gas-to-liquid mass flow ratio (GLR). Based on the low stoichiometry required for the gasification reaction, the burner nozzle must be operated at GLR ≤ 1 [2,3]. For the optimization of the atomization process under relevant conditions for EFG and scale-up of burner nozzles, it is essential to gain fundamental knowledge concerning atomization behavior at high system pressures [4].

In this study, the influence of gas velocity, system pressure, and nozzle geometry on spray formation is investigated for varying GLRs, concerning droplet size and jet breakup. The study aims to develop a system pressure scaling approach for external-mixing, twin-fluid atomizers based on gas momentum flow.

Many investigations concerning primary breakup and resulting spray quality in terms of Sauter mean diameter at atmospheric system pressure are reported in the literature by Marmottant and Villermaux [5], Hede et al. [6] and Faragò and Chigier [7] applying coaxial gas-assisted atomizers. A morphological study on primary jet breakup was performed by Faragò and Chigier [7] for water applying different nozzle geometries. As a result, the different breakup regimes were classified with regard to Re_{liq} and We_{aero}, as per Eqs. (1) and (2):

$$Re_{liq} = \frac{D_{liq} \cdot v_{liq} \cdot \rho_{liq}}{\eta_{liq}} \tag{1}$$

$$We_{aero} = \frac{\left(v_{gas} - v_{liq}\right)^2 \cdot \rho_{gas} \cdot D_{liq}}{\sigma} \tag{2}$$

with liquid jet diameter (D_{liq}), velocity (v), density (ρρ), dynamic viscosity (η), and surface tension (σ) as relevant process parameters. The subscripts *gas* and *liq* denote the gas and liquid phases, respectively. For increasing We_{aero}, the primary breakup regimes of a liquid jet change from Rayleigh-type breakup to membrane-type breakup and finally fiber-type breakup. The latter can be devided into the submodes pulsating and superpulsating as described in detail by Faragò and Chigier [7]. The effect of dynamic pressure ratio (in the following called momentum flux ratio) of the gas and liquid phase, according to Eq. (3), was added in a later

* Corresponding author at: Hermann-von-Helmholtz Platz 1, 76344 Eggenstein-Leopoldshafen, Germany.
E-mail address: simon.wachter@kit.edu (S. Wachter).

https://doi.org/10.1016/j.jaecs.2020.100019
Received 20 July 2020; Received in revised form 19 November 2020; Accepted 19 November 2020
Available online 28 November 2020

investigation by Lasheras and Hopfinger [8].

$$j = \frac{j_{gas}}{j_{liq}} = \frac{v_{gas}^2 \cdot \rho_{gas}}{v_{liq}^2 \cdot \rho_{liq}} \quad (3)$$

As the nozzle geometry and gas density were kept constant in the investigations by Lasheras and Hopfinger [8], the results on the primary breakup length and spray angle were assigned only on the basis of the momentum flux ratio, which is therefore only a function of the gas phase velocity. Moreover, the momentum flow ratio as outlined in Eq. (4), is often used for spray characterization [9–12].

$$J = \frac{J_{gas}}{J_{liq}} = \frac{v_{gas}^2 \cdot \rho_{gas} \cdot A_{gas}}{v_{liq}^2 \cdot \rho_{liq} \cdot A_{liq}} \quad (4)$$

Typically, investigations of twin-fluid atomization explain the influence of gas velocity on the primary breakup and droplet size distribution by changing the gas mass flow and thereby, the GLR. The increase in gas velocity generally leads to a decrease in droplet size across the entire spray cone [13,14] due to an increase in the aerodynamic forces. The influence of the gas velocity and GLR on the droplet size decreases at GLR >> 1, as reported by many researchers [15–17].

Several authors have studied the influence of system pressure on the resulting spray with respect to droplet size [18–23]. Reducing the literature overview on publications, which aim for the scaling of twin-fluid atomizers yields the following. Jakobs et al. [24] investigated the influence of the absolute system pressure on the resulting droplet size of a water spray between a p_{sys} = 1 – 21 bar for one nozzle at constant We_{aero}. To achieve a constant aerodynamic Weber number with increasing system pressure (i.e., ρ_{gas}), the gas velocity at the nozzle orifice was reduced. This led to an increase in the droplet size at higher system pressures and constant We_{aero}, and thus to the conclusion that the gas velocity is an essential parameter in the scaling of twin-fluid atomizers. Continuing these experiments, Sänger et al. [25] investigated the influence of system pressures between p_{sys} = 1–21 bar at constant gas velocity and different liquid viscosities (η_{liq} = 1–400 mPa•s) by applying one nozzle. Here, with increasing system pressure, the gas mass flow (i.e., GLR) was increased to keep the gas velocity constant. This approach led to a finer spray i.e., decreased droplet size with increase in the system pressure, owing to the increase in the aerodynamic forces. Additionally, for increasing j_{gas}, different dependencies of the resulting droplet size on system pressure and gas velocity were detected at η_{liq} = 100 mPa•s. Sänger [26] explained this by the influence of different induced liquid instabilities on the corresponding primary breakup morphology. To investigate the influence of system pressure at constant GLR, gas mass flow, and gas velocity, Wachter et al. [27] performed experiments at p_{sys} = 1–16 bar using pressure adapted twin-fluid atomizers. To increase the system pressure, the annular gap width (s_{gas} = 0.35–2.88 mm) was reduced to achieve constant operating conditions with respect to gas and liquid velocities and mass flows at the nozzle orifice, independent of the system pressure. As a result, for low system pressures (p_{sys} < 6 bar), a slight decrease in droplet size was detected owing to the higher aerodynamic forces. For higher system pressures, a sharp increase in the resulting droplet size was detected. The small gas gap width resulted in a fast deceleration of the gas phase, even close to the nozzle orifice, due to the entrainment of the gas phase. This investigation revealed the significant influence of the gas gap width on the resulting droplet size.

Further qualitative investigations of changes in the gas gap width s_{gas} were performed by Zhao et al. [28] at atmospheric system pressure in the range of s_{gas} = 1.9–10 mm and j = 0.01–620 using a high-speed camera. As a result, the authors represented a breakup regime classification depending on a modified momentum flux ratio j_m and aerodynamic Weber number We_m, as shown in Eqs. (5) and (6), below.

$$j_m = \frac{j}{1 + 50 \cdot \frac{A_{liq}}{A_{gas}}} \quad (5)$$

$$We_m = \frac{We}{1 + 1.4 \cdot \frac{A_{liq}}{A_{gas}}} \quad (6)$$

Leroux et al. [29,30] published research on the scaling of twin-fluid atomizers at atmospheric system pressure. These investigations were categorized into the nozzle nearfield (dense core zone) [29] and nozzle farfield (diluted zone) [30]. Applying several twin-fluid atomizers, the liquid jet diameter was varied between D_{liq} = 0.4–2 mm and the gas gap width between s_{gas} = 0.25–3.5 mm. Investigations of the dense core zone of the liquid jet were performed with a shadowgraph system to determine the breakup regimes as per Lasheras et al. [8] and correlations for the liquid core length and spray angle were derived depending on the momentum flux ratio j. The measurements led to the conclusion that the liquid core length is not a function of the spray regime and decreases with increasing momentum flux ratio. In contrast, the spray angle depends on the spray regime. The angle first increases within the fiber-type pulsating submode, whereas a further increase in j leads to a decrease within the superpulsation submode [29]. Measurements of droplet size distributions in the diluted spray zone were performed with a Phase Doppler Analyzer (PDA) at different axial positions (z = 14, 42, and 140 mm) and radially from −20 mm < x < 20 mm. As a result, two correlations for the pulsating and superpulsating submodes are presented, leading to the conclusion that the droplet size increases as D_{liq} increases and decreases with higher v_{gas} [30]. An approach considering increased mass flows, for twin-fluid atomizer scaling was not outlined.

As the literature review shows, no scaling approach considering increased system pressure for twin-fluid nozzles has been reported by previous investigations. Furthermore, empirical correlations for the calculation of the resulting droplet size at increased system pressure for variations in the parameters forming J_{gas} have not been derived. In summary as per past research, the gas velocity at the nozzle orifice and the gas orifice area (i.e., the gas gap width) have a distinct influence on the resulting droplet size of twin-fluid atomizers.

Therefore, this work investigates the influence of gas velocity, system pressure, and gas gap width on spray formation. A high-speed camera was used to detect the primary breakup and PDA for measuring the local droplet velocity and size. Three different nozzles with a constant liquid jet diameter but varying gas gap widths were operated at increased system pressure and constant gas velocity. To achieve a constant gas velocity with increasing system pressure, the gas mass flow was increased. Experiments were performed with three different gas velocities at each system pressure level. An empirical model for the calculation of the resulting droplet size at varying system pressure, depending on fitting parameters and gas momentum flow J_{gas} was developed based on the experimental results. This model allows for the system pressure scaling of twin-fluid atomizers in the investigated range of J_{gas}.

2. Experimental setup

As described by Wachter et al. [27], the experimental setup consists of the pressurized atomization test rig (PAT), a PDA and a high-speed camera. Three external-mixing twin-fluid atomizers having identical liquid orifice area, but different gas orifice area (varying gas gap width) were used to atomize water with pressurized air.

A schematic and a horizontal cross-sectional view (A-A) of the PAT spray test rig with an exhaust air system is shown in Fig. 1. The pressure chamber has an internal diameter of 300 mm and a total height of 3000 mm. It is designed for operation at system pressures up to p_{sys} = 21 bar. The external-mixing twin-fluid atomizer is mounted on the axially (z-direction) movable twin-fluid lance, which is fed by one of the two eccentric screw pumps with liquids featuring viscosities up to η_{liq} = 1000 mPa·s. The liquid mass flow can be controlled in the range of P1: $\dot{M}_{liq}$ = 10–60 kg·h^{-1} / P2: $\dot{M}_{liq}$ = 60–200 kg·h^{-1} using different screw pumps. The liquid mass flow and density were measured using a Coriolis flow meter with an uncertainty of < 0.5%. The com-

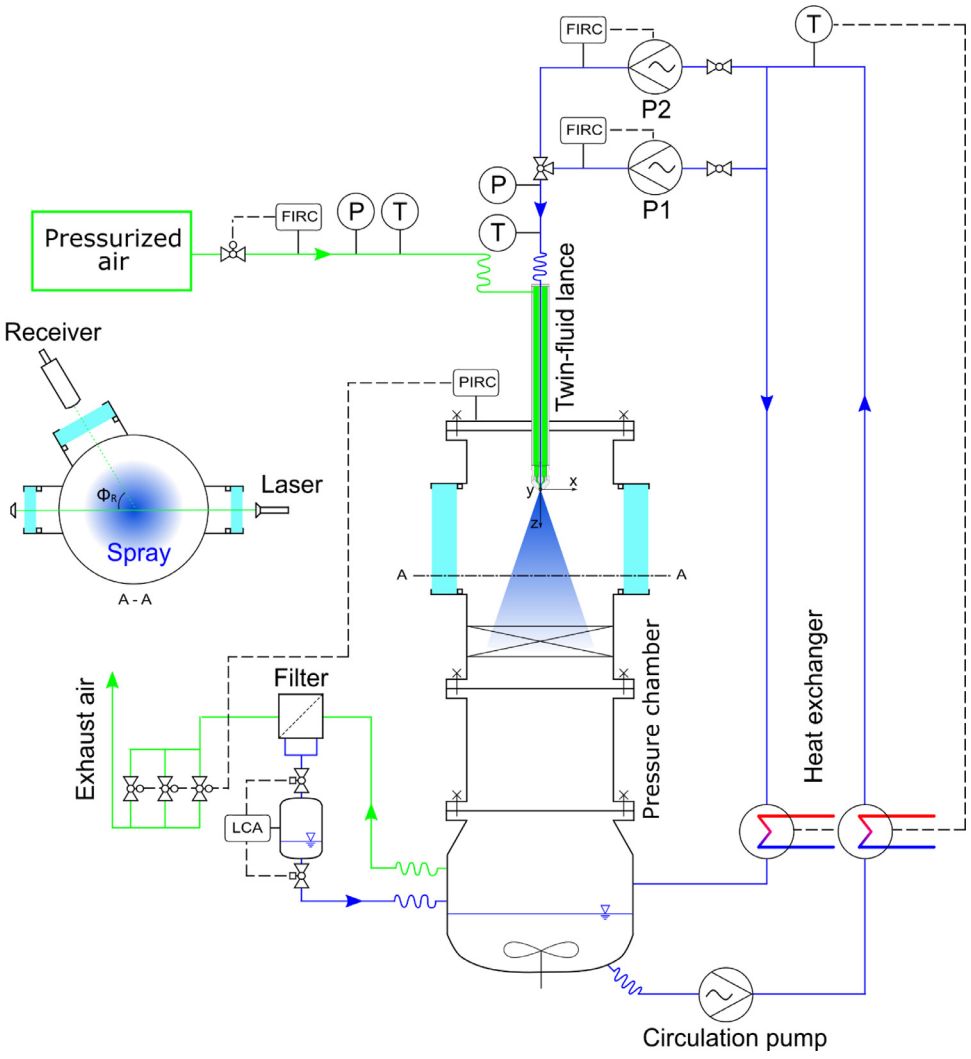

Fig. 1. Schematic of the experimental setup – Pressurized Atomization Test Rig (PAT).

pressed air volume flow V_{gas} was measured by a turbine meter with a measuring range of V_{gas} = 0.85–25 $m^3 \cdot h^{-1}$ and uncertainty of < 0.5%. A recalculation of the volume to the mass flow was performed using the measured local gas temperature and pressure at the turbine. To ensure well-defined nozzle inlet conditions, the liquid temperature can be adjusted in the range of T = 10–50 °C. The test rig is equipped with three high-quality glass windows that allow for optical access to the spray chamber. Two optical ports are located at Φ_R = 0° and 70° to enable Phase Doppler measurements in scattering mode with the highest intensity (first-order refraction) [31]. The third optical port is positioned at Φ_R = 180° to allow for spray investigations in backlight mode with optical measurement system. A flow straightener (honeycomb structure) is located below the measuring plane to avoid influences on the measurement owing to the recirculation of droplets into the region of interest.

All investigations were conducted with 3 external-mixing twin-fluid nozzles, as shown in Fig. 2. The liquid (blue) was supplied through a circular central tube (D_{liq} = 2 mm) at the nozzle axis. D_{liq} was kept constant for all nozzles. The liquid jet was surrounded by a coaxial gas stream (green), the width of the gas gap was adjusted between s_{gas} = 0.6–2.0 mm, as listed in Table 1. The nozzle has parallel flow channels in order to avoid disturbance of the liquid jet owing to the gas flow angle and turbulence effects. In addition, the influence of the tube separating the gas and liquid at the nozzle orifice was minimized by reducing the wall thickness b to 0.1 mm. This configuration results in an undisturbed gas flow at the exit of the nozzle [32].

Table 1
Nozzle data (Nozzle 1–3) with similar geometry and varying gas gap widths s_{gas}.

	D_{liq} in mm	s_{gas} in mm	D_{gas} in mm	A_{gas} in mm^2
Nozzle 1	2.00	2.00	6.20	26.42
Nozzle 2	2.00	1.20	4.60	13.02
Nozzle 3	2.00	0.60	3.40	5.25

A high-speed camera for the qualitative observation of the primary breakup of the liquid jet was utilized in the nozzle nearfield. The camera features a frame rate of 3.6 kHz operation at 1024 × 1024-pixel resolution and frame rates of up to 500 kHz at reduced resolution. A lens with a focal length of f_{HG} = 105 mm was used to capture primary breakup morphologies. In this study, the frame rate was set to 7.5 kHz at a reduced resolution of 768 × 640 pixel. Thus, the images have dimensions of 41.4 × 34.4 mm^2 with a spatial resolution of 54 $\mu m \cdot pix^{-1}$. The images were captured through backlight illumination of the region of interest with a special lighting setup. An array of 9 high-power light-emitting diodes (LEDs) with a total luminous flux of 9 × 4500 lm was used. The position of each single LED within the LED array was optimized to achieve the best possible light distribution. Owing to the high intensity and homogeneous distribution of the light, very short exposure times (t_{Exp} ~ 7 µs) were employed. This light setup allowed for a sharp representation of droplets even at fast flow conditions. To ensure

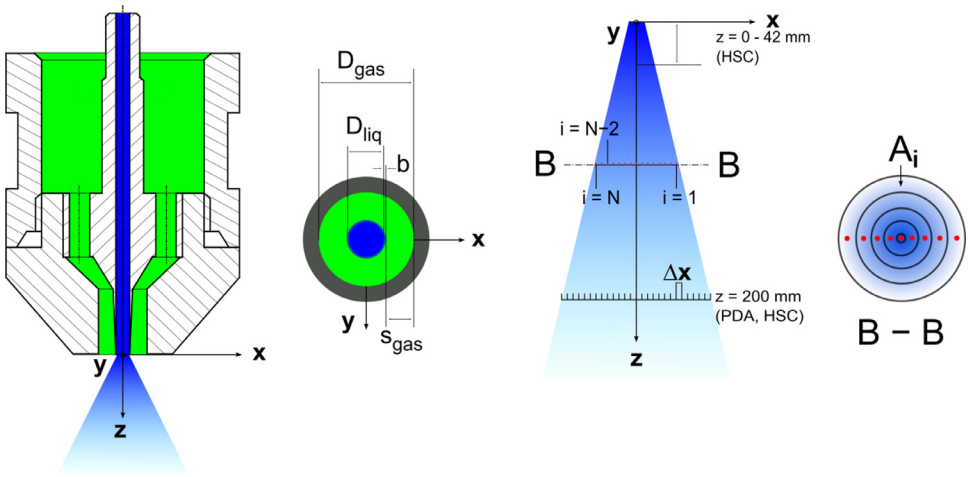

Fig. 2. Scheme of the external-mixing twin-fluid nozzle.

Table 2
Settings of the fiber PDA evaluated by the sensitivity analysis.

Parameters	Values	Unit	Parameters	Values	Unit
Transmitter focal length f_T	1000	mm	Laser wavelength λ_L	561	nm
Receiver focal length f_R	1000	mm	Laser power (transmitter exit)	40	mW
Beam expander ratio E	1	–	Off-axis angle Φ_R	70	°
Receiver slit width (physical) l_S	200	µm	Frequency shift f_Λ	80	MHz

appropriate recording of representative data of the liquid disintegration process, a set of at least 2000 high-speed images was recorded at every operating condition along with a background reference image without liquid flow.

For the observation of single droplets within the spray at $z = 200$ mm from the nozzle orifice, also the high-speed camera was applied. In addition, the same camera was used: (i) to optimize the PDA hardware settings (receiver mask); (ii) for sphericity check of the droplets in the measuring plane to ensure reliable PDA data; (iii) to qualitatively confirm the tendencies measured by the PDA; and (iv) as a validation tool for the PDA data in order to eliminate deviations arising out of the Gaussian beam effect [33]. For the detection of droplets across the entire spray cone, 10 000 images were recorded over the radial measurement area $x = \pm 44$ mm at $z = 200$ mm downstream of the nozzle orifice in the measuring plane. The largest measurement error concerning droplet size was $\Delta d_p < 30$ µm. Because the droplet measurement with the high-speed camera setup was only used for qualitative investigations of large droplets, the accuracy was considered to be adequate. Droplets without detectable contours were rejected from recording.

The droplet size and velocity were measured at a high spatial and temporal resolution within the spray cone using a fiber PDA and SprayExplorer system by Dantec Dynamics. For data collection, the PDA was operated in a forward scattering arrangement and refraction mode (1st order). The receiver was set to off-axis angle of $\Phi_R = 70°$. A slit with a length of $l_S = 200$ µm was used in order to (i) obtain a well-defined detection volume dimension; (ii) ensure high data rates under dense spray conditions; and (iii) to enable flux calculation. To guarantee the detection of large droplets and minimize sizing errors due to the Gaussian beam effect, lenses with a focal length of 1000 mm were used for both transmitter f_T and receiver f_R [33]. In addition, the asymmetric Mask B was chosen for the receiver to eliminate possible measurement errors due to the Gaussian beam effect (trajectory effect). With this optical configuration, the PDA system allows for the detection of water droplets with a minimum size of 1 µm and maximum size of 1357 µm [31]. To improve the PDA instrument settings with respect to small droplets (e.g., data rate and validation rate), the optimum PDA user settings were evaluated in advance by a sensitivity study [34]. The final PDA settings are displayed in Table 2.

To enable drop size measurements at different positions within the spray cone, a receiver and transmitter were mounted on a 3D traverse system, which guarantees spatial reproducibility of < 0.1 mm. Data were obtained by moving the detection volume relative to the nozzle position. The measurements were taken at several radial (traverse along the x-axis) positions with a radial increment of $\Delta x = 2$–4 mm, depending on the position in the spray. The axial droplet velocity component v_z was measured using the orientation of the coordinate system, as indicated in Fig. 2, and the alignment of the fringes of the laser beam couple ($\lambda_L = 561$ nm – yellow). To ensure a reliable database for every radial position during the PDA measurements, the sample size was set to 50 000 droplets. For the outermost radial measuring position, a sample size of 50 000 droplets was not reached under all operating conditions. Nevertheless, at least 5000 droplets were detected at the boundary of the spray cone, which is still a statistically reliable number [26]. The raw data from the manufacturer software were used to compute the arithmetic mean, statistical data, and additional information (i.e., mass flux and $ID_{32,m}$) using the toolbox *SprayCAT* [26]. For the global characterization of the spray, a global characteristic diameter was computed i.e., a mass-weighted integral Sauter mean diameter ($ID_{32,m}$) including all measurement positions of a radial profile, at a fixed axial position z. The integral Sauter mean diameter $ID_{32,m}$ was calculated according to Eq. (7) and based on the local volume mean diameter $D_{30,i}$ and local surface mean diameter $D_{20,i}$. These diameters were weighted by the local mass flux $\dot{m}_i$ and the annulus area A_i (see Fig. 2), corresponding to the measurement position i along the radial axis $x_1 \le x_i \le x_N$ with N measurement positions. The outermost point x_N for each operating condition was set to $x = \pm 44$ mm.

$$ID_{32,m} = \frac{\sum_{i=1}^{N} D_{30,i}^3 \dot{m}_i A_i}{\sum_{i=1}^{N} D_{20,i}^2 \dot{m}_i A_i} \tag{7}$$

Further information regarding the computation of the global size distribution and drop size moments can be obtained from DIN SPEC 91,325 [35], and Albrecht [31]. The mass flux $\dot{m}_i$ was calculated from the PDA data according to Albrecht [31], using the *SprayCAT* toolbox. All PDA measurements were conducted at an axial distance of $z = 200$ mm from the nozzle orifice and repeated at least 3 times. For each operating condi-

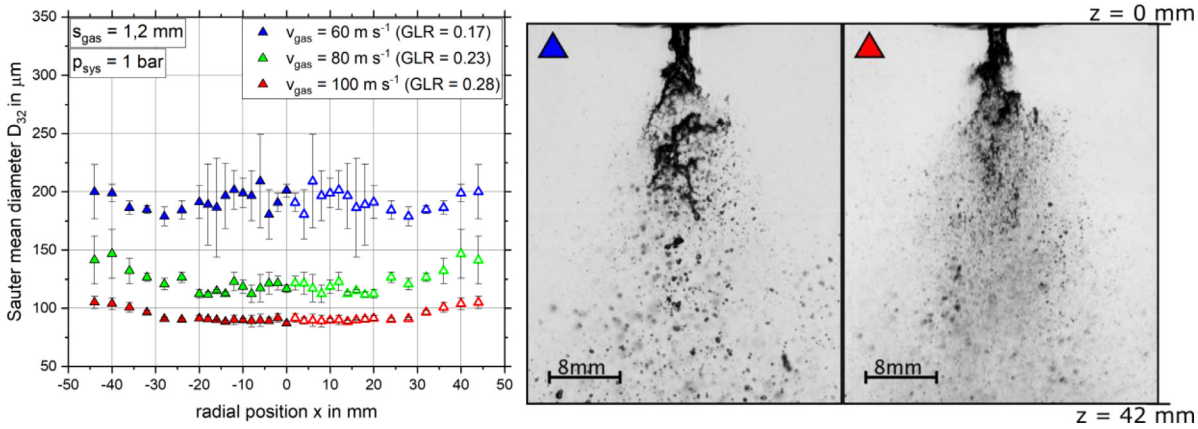

Fig. 3. Radial distribution of the Sauter mean diameter at z = 200 mm with s_{gas} = 1.2 mm as a function of the gas velocity at p_{sys} = 1 bar (open symbols denote mirrored positions); High-speed camera images of primary jet breakup at p_{sys} = 1 bar and v_{gas} = 60 m·s^{-1} (left) / v_{gas} = 100 m·s^{-1} (right).

Table 3
Operating conditions of the experiments.

	s_{gas} in mm	s_{gas} in mm	s_{gas} in mm
	2.0	1.2	0.6
	v_{gas} in m·s^{-1}	v_{gas} in m·s^{-1}	v_{gas} in m·s^{-1}
	60 / 80 / 100	60 / 80 / 100	60 / 80 / 100
p_{sys} in bar	$\dot{M}_{gas}$ in kg·h^{-1}	$\dot{M}_{gas}$ in kg·h^{-1}	$\dot{M}_{gas}$ in kg·h^{-1}
1	6.9 / 9.2 / 11.5	3.4 / 4.5 / 5.6	- / - / -
3	20.7 / 27.6 / 34.5	10.2 / 13.5 / 16.8	4.1 / 5.6 / 6.9
6	41.4 / 55.2 / 69.0	20.4 / 27.0 / 33.6	8.2 / 11.1 / 13.8
11	75.9 / 101.2 / -	37.4 / 49.5 / 61.6	15.1 / 20.4 / 25.3
16	- / - / -	54.4 / 72.0 / 89.6	21.9 / 29.6 / 36.8
21	- / - / -	71.4 / 94.5 / -	28.8 / 38.9 / 48.3

tion and nozzle, the rotational symmetry of the spray cone was checked, taking a full radial profile in the first set of experiments. After the rotational symmetry was proven, the following repetition measurements were performed taking half-profiles from the spray edge to the center at x = 0 mm. The results of these sets of experiments were then mirrored to obtain full profiles. Therefore, the following figures show all radial Sauter mean diameter distributions as mirrored profiles at x = 0 mm, while the plotted and mirrored data points are shown as open symbols.

3. Results and discussion

In order to investigate the influence of (i) gas velocity v_{gas}, (ii) system pressure p_{sys} and (iii) gas gap width s_{gas} on primary breakup and resulting droplet size at a constant liquid mass flow of $\dot{M}_{liq}$ = 20 kg·h^{-1}, the three nozzles described in Table 1 were subjected to three different gas velocities and six different system pressures. The operating conditions for all the measurements are presented in Table 3. In all experiments, pressurized air at T = 20 °C was used as atomization agent. The supplied water was maintained at T = 20 °C. All PDA measurements were performed at an axial distance of z = 200 mm downstream of the nozzle exit. The dashed operation points in Table 3 indicate a spray beyond the scope of the PDA measuring system because of the detectable droplet size being out of range and shading effects.

(i) Influence of gas velocity on Sauter mean diameter at constant system pressure and gas gap width

In this section, the results regarding the influence of the gas velocity on the local Sauter mean diameter profiles at constant system pressure and gas gap width are discussed. The gas velocity was changed by varying the gas mass flow (i.e., GLR). The results for the nozzle with a slit width of s_{gas} = 1.2 mm at a p_{sys} = 1 bar are shown in Fig. 3 (left). Furthermore, high-speed camera images of primary jet breakup under these operating conditions are presented in Fig. 3 (right) for v_{gas} = 60 m·s^{-1} and v_{gas} = 100 m·s^{-1}.

The PDA data in Fig. 3 show that an increase in the gas velocity (i.e., GLR) leads to a decrease in the Sauter mean diameter. This is in accordance with the findings reported in the literature [15,36]. This tendency is identified for each system pressure and all the nozzles under investigation. This can be explained by an increase in the aerodynamic force of the gas phase (with increasing gas velocity, i.e., GLR), leading to improved disintegration of the liquid jet and liquid fragments. For the maximum gas velocity of v_{gas} = 100 m·s^{-1}, the produced spray is homogeneous (see high-speed camera image in Fig. 3 (right)), which corresponds to the measured radial profile with small standard deviations. Larger Sauter mean diameters were detected at the spray boundary due to smaller aerodynamic forces in this area. For a low gas velocity (v_{gas} = 60 m·s^{-1}), larger fragments even farther downstream from the nozzle orifice were detected. This results in a radial D_{32}-profile with a higher standard deviation (see Fig. 3 (left)). The effect of gas velocity on the Sauter mean diameter decreases with increasing system pressure, owing to the already significantly high aerodynamic forces at increased system pressure, as discussed in the following section.

(ii) Influence of system pressure on Sauter mean diameter at constant gas velocity and gas gap width

This section focuses on the influence of system pressure (i.e., gas density) on the local Sauter mean diameter profiles at constant gas velocity and gas gap width. The change in system pressure at constant gas velocity for constant nozzle geometry leads to an increase in the gas mass flow (i.e., GLR) owing to the higher gas density. The results of the nozzle with a slit width of s_{gas} = 1.2 mm at v_{gas} = 60 m·s^{-1} are shown in Fig. 4 (left). In addition, high-speed camera images of primary jet breakup under these operating conditions are presented in Fig. 4 (right) for p_{sys} = 1 bar and p_{sys} = 21 bar.

An increase in the system pressure at constant gas velocity results in an increase in the GLR. For $s_{gas} \geq$ 1.2 mm and v_{gas} = 60–100 m·s^{-1}, the increase in the system pressure results in smaller Sauter mean diameters for all radial positions and a more homogeneous spray without larger droplet size deviations. The system pressure dependency of the Sauter mean diameter decreases with increasing system pressure until p_{sys} = 11 bar (s_{gas} = 1.2 mm), which can be seen in Fig. 4 and is consistent with findings reported in the literature [9,18,26]. This dependency can also be determined for s_{gas} = 0.6 mm at v_{gas} = 80–100 m·s^{-1} and s_{gas} = 2 mm at v_{gas} = 60–100 m·s^{-1}.

High-speed camera images confirm these measurements, as shown in Fig. 4. Both operating conditions are in the fiber-type breakup mode,

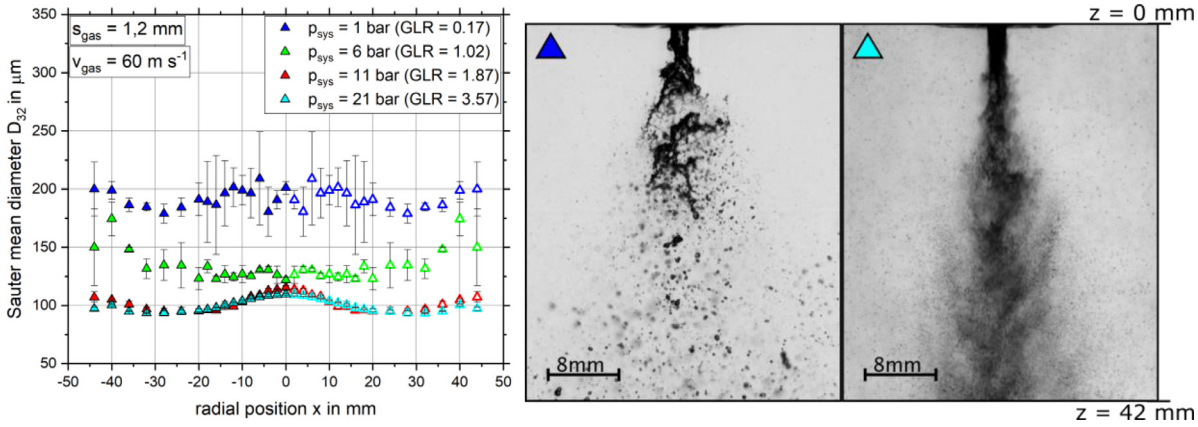

Fig. 4. Radial distribution of the Sauter mean diameter at $z = 200$ mm with $s_{gas} = 1.2$ mm as a function of the system pressure at $v_{gas} = 60$ m·s^{-1} (the open symbols denote the mirrored positions); High-speed camera images of the primary jet breakup at $v_{gas} = 60$ m·s^{-1} and $p_{sys} = 1$ bar (left) / $p_{sys} = 21$ bar (right).

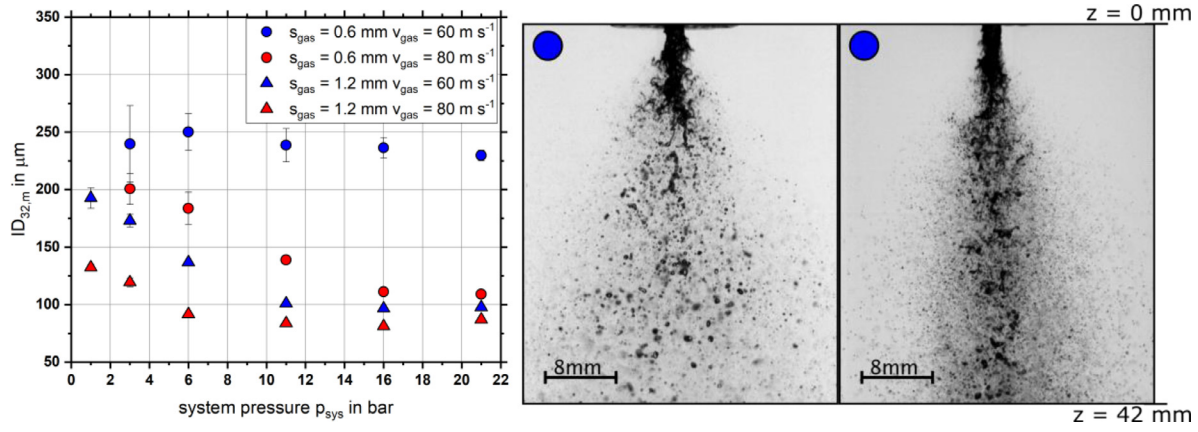

Fig. 5. Mass-weighted integral Sauter mean diameter at $z = 200$ mm with $s_{gas} = 1.2$ mm and $s_{gas} = 0.6$ mm as a function of the system pressure for $v_{gas} = 60$ m·s^{-1} and $v_{gas} = 80$ m·s^{-1}; High-speed camera images of the primary jet breakup applying $s_{gas} = 0.6$ mm and $v_{gas} = 60$ m·s^{-1} at $p_{sys} = 3$ bar (left) and $p_{sys} = 21$ bar (right).

according to [7]. Here, the disintegration at increased system pressure leads to the formation of a homogeneous spray with an increased droplet number density. This is caused, due to the higher aerodynamic forces and increased gas mass flow (i.e., GLR).

For $s_{gas} = 0.6$ mm and $v_{gas} = 60$ m·s^{-1}, only a negligible influence of the system pressure on the resulting Sauter mean diameter was observed between the $p_{sys} = 3$–21 bar (Fig. 5 (left)). To gain a deeper insight, Fig. 5 (right) shows the corresponding high-speed camera images at $p_{sys} = 3$ bar and $p_{sys} = 21$ bar, which both reveal a fiber-type breakup. As illustrated, at increased system pressure the formation of tiny droplets, at the boundary of the spray cone, out of the fibers improves. After the primary breakup, the gas velocity is decelerated owing to the entrainment of the surrounding gas phase, inhibiting further breakup via secondary atomization. Therefore, large droplets are detected by the PDA, leading to an almost constant Sauter mean diameter and only a slight reduction with increasing system pressure for the nozzle with $s_{gas} = 0.6$ mm and $v_{gas} = 60$ m·s^{-1}.

The influence of system pressure on the droplet size for different gas gap widths shows that with increasing s_{gas}, the plateau of the Sauter mean diameters is reached at lower system pressures.

One explanation of this finding can be given by the theory of a gas-free jet. A free jet can be described as a shear flow into free space, where the gas jet is in contact with quiescent air. Owing to the velocity gradient, surrounding gas entrains the emerging jet, whereby the moving mass increases in conjunction with a decrease in velocity, while the overall momentum is conserved [37].

Here, a decrease in the gas orifice area (i.e., s_{gas}) leads to lower values of the gas velocity at the same distance to the nozzle orifice. This deceleration in the gas velocity can be explained by the entrainment of ambient gas into the atomization gas jet emerging from the nozzle, according to the free jet theory. This effect was studied in detail for similar atomizers at various s_{gas} values by Wachter et al. [27]. Additionally, the gas mass flow (i.e., GLR) is increased for wider gas gaps to keep the gas velocity constant, enhancing the previously discussed effect.

(iii) Influence of gas gap width on Sauter mean diameter at constant gas velocity and system pressure

In this section, the influence of the gas gap width on the local Sauter mean diameter profiles at constant gas velocity and system pressure is discussed. Increasing the gas gap width at constant gas velocity results in an increase in the gas mass flow (i.e., GLR) owing to the larger gas orifice area. The results of all three nozzles ($s_{gas} = 0.6$ / 1.2 / 2.0 mm) for $v_{gas} = 80$ m·s^{-1} and $p_{sys} = 3$ bar are shown in Fig. 6. In addition, high-speed camera images are also presented in Fig. 6 for $s_{gas} = 0.6$ mm (left) and $s_{gas} = 2.0$ mm (right).

As illustrated in Fig. 6 for $p_{sys} = 3$ bar and $v_{gas} = 80$ m•s^{-1}, an increase in the gas gap width (i.e., GLR) at a constant gas velocity and system pressure leads to a decrease in the Sauter mean diameter. A similar dependency was detected under all operating conditions investigated in this study. This can be explained by two effects: (i) for wider gas gaps, the gas phase emerging from the nozzle remains at a higher velocity over a longer distance from the nozzle orifice in accordance with the

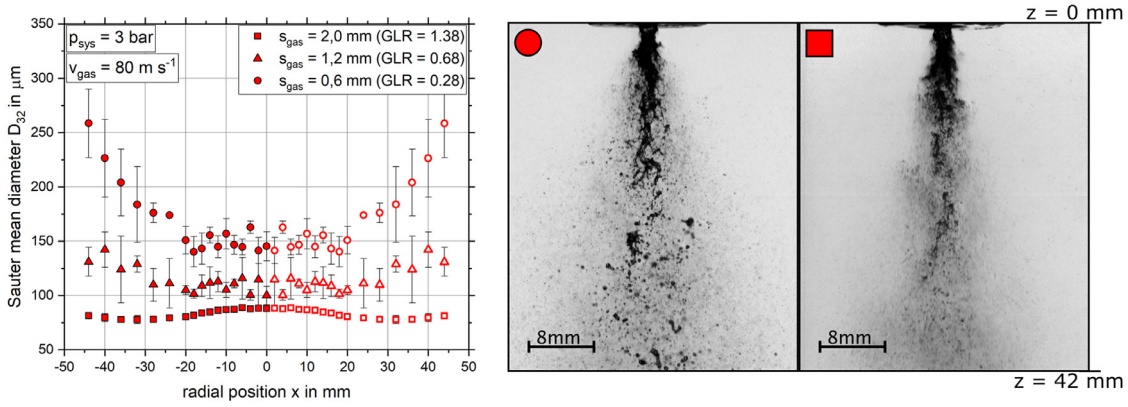

Fig. 6. Radial distribution of the Sauter mean diameter at $z = 200$ mm as a function of the gas gap width at $p_{sys} = 3$ bar and $v_{gas} = 80$ m·s^{-1} (open symbols denote mirrored positions); High-speed camera images of the primary jet breakup at $p_{sys} = 3$ bar and $v_{gas} = 80$ m·s^{-1} applying $s_{gas} = 0.6$ mm (left) and $s_{gas} = 2.0$ mm (right).

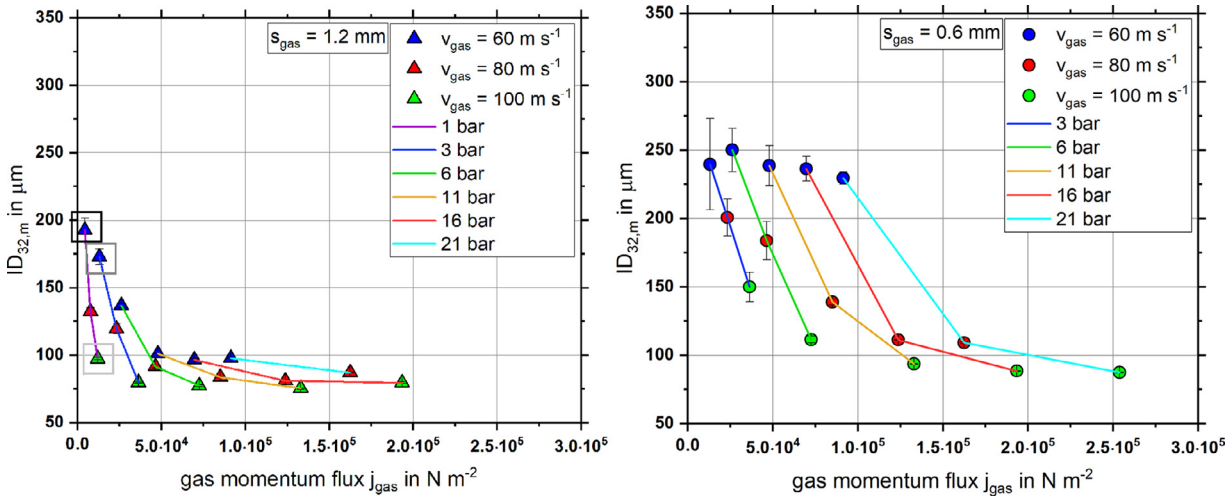

Fig. 7. Mass-weighted integral Sauter mean diameter at $z = 200$ mm as a function of gas momentum flux j_{gas} for different gas velocities and system pressures, applying $s_{gas} = 1.2$ mm (left) and $s_{gas} = 0.6$ mm (right).

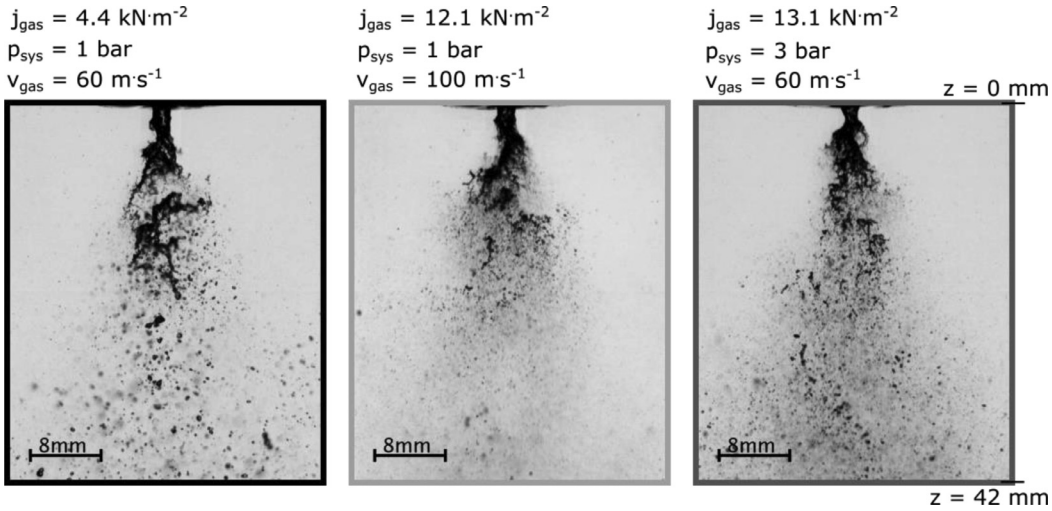

Fig. 8. High-speed camera images of the primary jet breakup applying $s_{gas} = 1.2$ mm at $p_{sys} = 1$ bar and $v_{gas} = 60$ m·s^{-1} (left), $p_{sys} = 1$ bar and $v_{gas} = 100$ m·s^{-1} (middle) and $p_{sys} = 3$ bar and $v_{gas} = 60$ m·s^{-1} (right).

free-jet theory; (ii) a higher gas mass flow leads to a higher aerodynamic force being available for the disintegration of the liquid jet. The discussed dependency is qualitatively proven by the high-speed camera images presented in Fig. 6 (right). The high deviations in the local Sauter mean diameter at s_{gas} = 0.6 mm can be explained by comparably large droplets across the entire spray cone. In contrast, the small deviations in the local Sauter mean diameter for s_{gas} = 2.0 mm can be explained by the homogeneity of the spray. As seen in the high-speed camera image for s_{gas} = 2.0 mm, no large liquid fragments remain in the spray, leaving the detection area at z = 42 mm. This is consistent with the results of Zhao et al. [28], where a morphological study of the primary breakup was presented, showing that an increase in the gas orifice area A_{gas} leads to a fiber-type breakup with small droplets and a more homogeneous spray.

In the literature, the momentum flux ratio j or the corresponding aerodynamic Weber number We_{aero} were used: (i) to scale nozzles within the investigated limits [29]; (ii) to describe the spray morphology [38]; or (iii) to explain the Sauter mean diameter dependencies [39]. The effect of the gas momentum flux on resulting $ID_{32,m}$ is discussed in the next section.

(iv) **Dependence of integral Sauter mean diameter on the gas momentum flux j_{gas}**

In order to compare the influence of gas velocity and system pressure on the integral, mass-weighted Sauter mean diameter for a distinct gas gap width, the gas momentum flux (i.e., We_{aero}) was used. The results of two different gas gap widths (s_{gas} = 1.2 mm, left and s_{gas} = 0.6 mm, right) at v_{gas} = 60–100 m·s^{-1} and p_{sys} = 1–21 bar are shown in Fig. 7. Here, each system pressure is represented by a specific colored line, whereas the same colored symbols represent a specific gas velocity.

With increasing gas momentum flux j_{gas}, the droplet size decreases for both the constant system pressure and constant gas velocity. This effect was observed for all gas gap widths, except for s_{gas} = 0.6 mm at v_{gas} = 60 m·s^{-1}. For a gas gap width of s_{gas} = 1.2 mm in Fig. 7 (left), the gas velocity at the nozzle orifice exhibits a greater influence on the droplet size compared to the system pressure. With increasing system pressure, the dependency of gas velocity decreases significantly, leading to a plateau in the droplet size for $j_{gas} > 5 \times 10^4$ N·m^{-2}. In contrast, for lower gas gap widths (s_{gas} = 0.6 mm), the influence of gas velocity on droplet size is even higher at increased system pressure and gas momentum flux.

Additionally, the influence of the gas velocity or system pressure on the droplet size can be discussed when changing the gas momentum flux by a fixed value [26]. As an example, Fig. 8 (left) shows the high-speed camera images of primary breakup with the gas momentum flux j_{gas} = 4.3 kN·m^{-2} under the conditions, s_{gas} = 1.2 mm, p_{sys} = 1 bar, and v_{gas} = 60 m·s^{-1}. When the gas momentum flux is increased by $\Delta j_{gas} \approx$ 8 kN·m^{-2}, different results are detected, using the system pressure or gas velocity for the increment of j_{gas}. The primary breakup of Fig. 8 (middle) results from changing the momentum flux by a variation in the gas velocity from v_{gas} = 60 m·s^{-1} to v_{gas} = 100 m·s^{-1}. In contrast, Fig. 8 (right) shows the primary breakup for the same gas momentum flux difference applied by a variation in system pressure from p_{sys} = 1 bar to p_{sys} = 3 bar. Comparing the results owing to variation in the gas velocity, and variation in system pressure, a difference in the spray characteristics can be seen from the high-speed camera images and is confirmed by the data plotted in Fig. 7 (left) (see gray colored frames in the diagram and corresponding high-speed camera images). The spray, resulting from the variation of j_{gas} through changes in gas velocity, is more homogeneous and results in smaller droplets. In contrast, the variation through changes in system pressure led to a slight reduction in droplet size, and several larger droplets remaining after completion of the primary atomization process.

(v) **Dependence of integral Sauter mean diameter on the gas momentum flow J_{gas} and scaling approach**

Table 4
Resulting parameters A, B and C as a function of the system pressure for p_{sys} = 3, 11 and 21 bar.

p_{sys} in bar	$A(p_{sys})$ in µm	B in N	$C(p_{sys})$ in µm
3	250	0.19	70
11	600	0.19	80
21	1500	0.19	90

Finally, the gas momentum flow J_{gas} is applied to interpret the experimental results as this variable includes all the investigated parameters (A_{gas}, v_{gas}, and ρ_{gas}). Fig. 9 (left) shows the results of $ID_{32,m}$ at different system pressures, p_{sys} = 3, 11, and 21 bar, considering all gas gap widths under investigation s_{gas} = 0.6 mm ● / 1.2 mm ▲ / 2.0 mm ■ and gas velocities at the nozzle orifice v_{gas} = 60 / 80 / 100 m·s^{-1}.

With increasing gas momentum flow J_{gas} at a constant system pressure, a decrease in the droplet size was observed owing to increase in the gas velocity and/or an increase in the gas gap width. Increments in system pressure at a constant gas momentum flow lead to an increase in droplet size because of a shift in either the gas gap width or gas velocity towards smaller values. For large gas momentum flows, the $ID_{32,m}$ FIT-curves exhibit a plateau at all system pressures, indicating that a further increase in the gas momentum flow causes only minor changes in the droplet size. At high GLR values (GLR >> 1), the same effect was observed by several authors at atmospheric system pressure [15–17].

With the objective of pressure scaling for external-mixing twin-fluid atomizers and considering the importance of the influence of gas momentum flow on Sauter mean diameter, an empirical model was derived to explain the droplet size behavior. The potential fit was chosen considering the shape of the plot of Sauter mean diameter results plotted as a function of the gas momentum flow (see Fig. 9 (left)). Eq. (8) shows the empirical model, which describes $ID_{32,m}$ as a function of system pressure and gas momentum flow.

$$ID_{32,m} = A(p_{sys}) \cdot e^{-\frac{J_{gas}}{B}} + C(p_{sys}) \tag{8}$$

For different system pressures, a constant variable B and two pressure-dependent parameters A and C were applied and correlated using a least-square method. The parameters for the pressure steps (as shown in Fig. 9) are listed in Table 4.

Based on the fact, that the parameters A and C are dependent on system pressure, Eqs. (9) and (10) are obtained.

$$A(p_{sys}) = 3.0 \cdot p_{sys}^2 + 220 \tag{9}$$

$$C(p_{sys}) = 1.1 \cdot p_{sys} + 67 \tag{10}$$

In order to demonstrate the accuracy of the model, a parity plot showing the measured versus calculated $ID_{32,m}$ values is shown in Fig. 9 (right). Across all measurement conditions, the parity plot shows good agreement between the calculated $ID_{32,m}$ and the measured values. The maximum deviation of 12.7% was observed for p_{sys} = 3 bar, v_{gas} = 100 m·s^{-1} and s_{gas} = 1.2 mm, leading to a difference of $\Delta ID_{32,m}$ = 11 µm.

To evaluate this model with respect to the calculated integral Sauter mean diameters against different system pressures, the measurements of droplet size at p_{sys} = 6 and 16 bar (as shown in Fig. 10 as a function of the gas momentum flow and plotted as dots) were used as assessment criteria. The curves representing the model approach (see Eqs. (8), (9), and (10)) for the respective system pressures are plotted as lines. For all of the assessment criteria, the deviation is below 12% except for the point at p_{sys} = 6 bar and J_{gas} = 0.69 N, where the deviation is $\Delta ID_{32,m}$ = 18 µm, which equals 22%.

The evaluation of the model for p_{sys} = 6 and 16 bar showed that the deviation between the calculated and measured $ID_{32,m}$ values is small and generally within the accuracy at low J_{gas}. As a result, the applica-

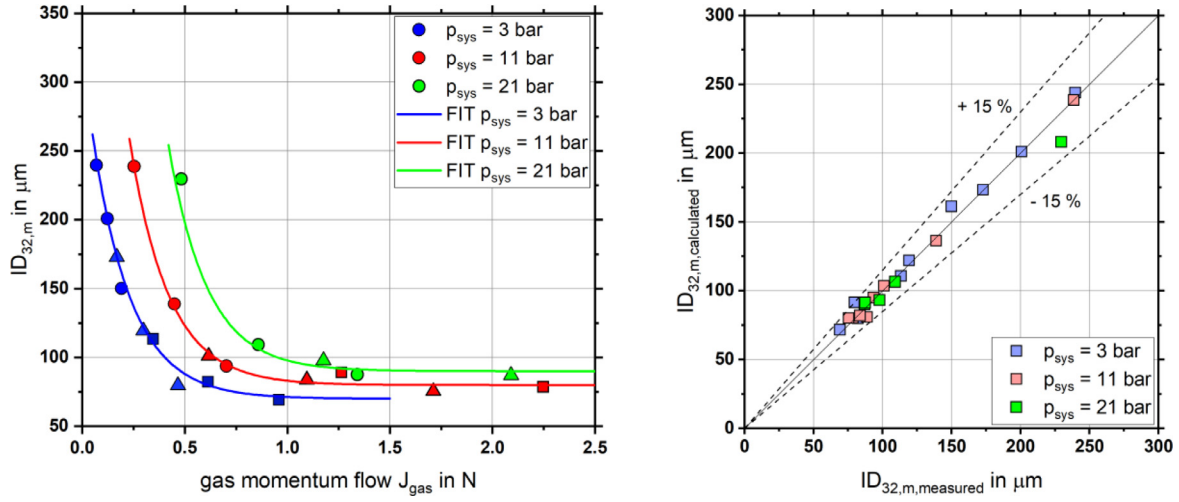

Fig. 9. Mass-weighted integral Sauter mean diameter at $z = 200$ mm as a function of gas momentum flow J_{gas} for different system pressures, applying different gas gap widths (s_{gas} = 0.6–2.0 mm) and gas velocities (v_{gas} = 60–100 m·s^{-1}). As lines, an empirical model is presented for different system pressures (left). Parity plot comparing the calculated $ID_{32,m}$ via an empirical model with the measured $ID_{32,m}$ (right).

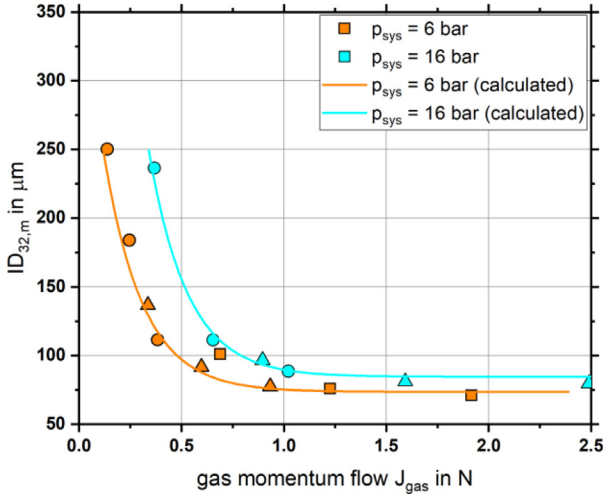

Fig. 10. Mass-weighted integral Sauter mean diameter at $z = 200$ mm as a function of the gas momentum flow J_{gas} for different system pressures, applying different gas gap widths (s_{gas} = 0.6–2.0 mm) and gas velocities (v_{gas} = 60–100 m·s^{-1}). The lines indicate the results of the empirical model for system pressures p_{sys} = 6 bar and 16 bar.

bility of the model for system pressures between p_{sys} = 1–21 bar and J_{gas} = 0.07–2.5 N is proven for $\dot{M}_{liq}$ = 20 kg·h^{-1}.

Extrapolations of the model approach towards higher system pressures, as commonly applied in EFG (i.e., p_{sys} = 40 or 80 bar), allow for an estimation of the expected droplet size.

Conversely, to achieve a specific droplet size, the nozzle gas orifice area and the required operating conditions can be calculated as follows: (i) for a requested $ID_{32,m}$ value and a given system pressure, the necessary gas momentum flow is calculated by means of the empirical correlation (see Eq. (8)); (ii) with a required GLR for the demanded process conditions, the related gas velocity, and thereby, the gas gap width for the twin-fluid atomizer is obtained.

4. Conclusion

This study investigated the influence of system pressure, gas velocity, and gas gap width on spray quality (D_{32}, $ID_{32,m}$) for twin-fluid atomizers operated at liquid mass flow of $\dot{M}_{liq}$ = 20 kg·h^{-1}. The nozzle geometry was kept similar, except that the gas gap width was changed. At every system pressure level between p_{sys} = 1–21 bar, three different gas velocities (v_{gas} = 60 / 80 / 100 m·s^{-1}) were investigated by changing the gas mass flow (i.e., GLR). High-speed camera images were used to observe the primary breakup, and to explain local measurements of droplet size performed by a phase Doppler anemometer. Thereafter, the gas momentum flux as well as the gas momentum flow were applied to describe the atomization process. Finally, an empirical model was derived, enabling the system pressure scaling of twin-fluid atomizers for the range of gas momentum flow under investigation. The results of the experiments can be summarized as follows:

- Increasing the gas velocity leads to a decrease in the droplet size at a constant system pressure and gas gap width.
- Increasing the system pressure leads to a decrease in the droplet size at constant gas velocity and gas gap width. This effect was observed under all operating conditions except for the smallest gas gap width and low gas velocity. The droplet size was nearly constant with increase in the system pressure at smallest gas gap width and low gas velocity.
- Increasing the gas gap width leads to a decrease in the droplet size at constant gas velocity and system pressure.
- A distinct change in the gas momentum flux via either changes in the gas velocity or system pressure leads to different results in spray quality ($ID_{32,m}$). This indicates that the gas momentum flux alone is not sufficient for describing the spray quality at varying system pressures.
- By using the gas momentum flow for the characterization of atomization behavior, an empirical model was derived, which enables system pressure scaling across the investigated range of the gas momentum flow.

Declaration of Competing Interests

The authors declare that they have no known competing financial interests or personal relationships that could have appeared to influence the work reported in this paper.

Acknowledgments

The authors gratefully acknowledge the financial support of the Helmholtz Association of German Research Centers (HGF) in the context of the research program, Energy Efficiency, Materials and Re-

sources (EMR). The present work contributes to the Helmholtz Virtual Institute for Gasification TechnologyHVIGasTech (VH-VI-429). http://www.hvigastech.org/.

References

[1] Higman C, van der Burgt M. Gasification. Amsterdam, Boston: Gulf Professional Pub/Elsevier Science; 2008.
[2] Giuffrida A, Romano MC, Lozza G. Thermodynamic analysis of air-blown gasification for IGCC applications. Appl Energy 2011;88(11):3949–58.
[3] Fleck S, Santo U, Hotz C, et al. Entrained flow gasification Part 1: gasification of glycol in an atmospheric-pressure experimental rig. Fuel 2018;217:306–19.
[4] Carisson P, Gebart R, Grönberg C, et al. Spatially resolved measurements of gas composition in a pressurised black liquor gasifier. Environ Prog Sustain Energy 2009;28(3):316–23.
[5] Marmottant P, Villermaux E. On spray formation. J. Fluid Mech. 2004;498:73–111.
[6] Hede PD, Bach P, Jensen AD. Two-fluid spray atomization and pneumatic nozzles for fluid bed coating/agglomeration purposes: a review. Chem Eng Sci 2008;63:3821–42.
[7] Chigier N, Faragó Z. Morphological classification of disintegration of round liquid jets in a coaxial air stream. Atomization Sprays 1992;2(2):137–53.
[8] Lasheras JC, Hopfinger EJ. Liquid jet instability and atomization in a coaxial gas stream. Annu Rev Fluid Mech 2000;32(1):275–308.
[9] Rizk NK, Lefebvre AH. Spray characteristics of plain-jet airblast atomizers. ASME 1984;634(106).
[10] Xiao F, Dianat M, McGuirk JJ. LES of turbulent liquid jet primary breakup in turbulent coaxial air flow. Int J Multiphase Flow 2014;60:103–18.
[11] Engelbert C, Hardalupas Y, Whitelaw JH. Breakup phenomena in coaxial airblast atomizers. Proc R Soc Lond Series A: Math Phys Sci 1997;451(1941):189–229.
[12] Xia Y, Alshehhi M, Hardalupas Y, et al. Spray characteristics of free air-on-water impinging jets. Int J Multiphase Flow 2018;100:86–103.
[13] Hardalupas Y, Whitelaw JH. Characteristics of sprays produced by coaxial airblast atomizers. J Propulsion Power 1994;10(4):453–60.
[14] H. Lohner, C. Czisch, and U. Fritsching, “Impact of the gas nozzle arrangement on the flow field of a twin fluid atomizer with external mixing,”.
[15] Lefebvre AH. Twin-Fluid atomization Factors influencing mean drop size. Atomization Sprays 1992;2:101–19.
[16] Liu H-F, Li W-F, Gong X, et al. Effect of liquid jet diameter on performance of coaxial two-fluid airblast atomizers. Chem Eng Process 2006;45:240–5.
[17] Kim KY, Marshall WR Jr. Drop-Size Distributions from pneumatic atomizers. AlChE J 1971;17(3).
[18] T.U. Yu and J.M. Beér, “Secondary Atomization of coal-water fuel at elevated pressure, 1988″.
[19] Jasuja AK. Plain-jet airblast atomization of alternative liquid petroleum fuels under high ambient air pressure conditions. Am Soc Mech Eng 1982(3).
[20] Smith CF, Sojka PE, Lefebvre AH. Plain-Jet airblast atomization of coal-water slurry fuels. Warrendale, PA: SAE International; 1985.
[21] Mayer WOH. Coaxial atomization of a round liquid jet in a high speed gas stream: a phenomenological study. Exp Fluids 1994;16(6):401–10.
[22] Gullberg M, Marklund M. Spray characterization of twin fluid external mixing atomization of pyrolysis oil. Atomization Sprays 2012;22(11):897–919.
[23] Risberg M, Marklund M. Visualizations of gas-assisted atomization of black liquor and syrup/water mixtures at elevated ambient pressures. Atomization Sprays 2009:957–67.
[24] Jakobs T, Djordjevic N, Sänger A, et al. Influence of reactor pressure on twin-fluid atomization: basic investigations on burner design for high-pressure entrained flow gasifier. Atomization Sprays 2015;25(12):1081–105.
[25] Sänger A, Jakobs T, Djordjevic N, et al. Experimental investigation on the influence of ambient pressure on twin-fluid atomization of liquids with various viscosities. In: Proceedings of the 13th triennial international conference on liquid atomization and spray systems, Tainan, Taiwan, August 23-27, 2015 (ICLASS); 2015.
[26] A. Sänger, *Zerstäubung hochviskoser fluide bei variierendem systemdruck - Grundlagenforschung zur hochdruck-flugstromvergasung*, Dissertation, Karlsruher Institut für Technologie (KIT).
[27] Wachter S, Jakobs T, Kolb T. Experimental investigation on the influence of system pressure on resulting spray quality and jet breakup applying pressure adapted twin-fluid nozzles. Int J Multiphase Flow 2020;125.
[28] Zhao H, Liu H-F, Tian X-S, et al. Influence of atomizer exit area ratio on the breakup morphology of coaxial air and round water jets. AIChE J 2014;60(6):2335–45.
[29] Leroux B, Delabroy O, Lacas F. Experimental study of coaxial atomizers scaling. Part 1: dense core zone. Atomization Sprays 2007;17:381–407.
[30] Leroux B, Delabroy O, Lacas F. Experimental study of coaxial atomizers scaling. Part 2: diluted zone. Atomization Sprays 2007;17:409–30.
[31] Albrecht H-E. Laser doppler and phase doppler measurement techniques. Berlin, New York: Springer; 2003.
[32] Tian X-S, Zhao H, Liu H-F, et al. Effect of central tube thickness on wave frequency of coaxial liquid jet. Fuel Process Technol 2014;119:190–7.
[33] Araneo L, Damaschke N, Tropea C. Measurement and prediction of the Gaussian beam effect in the PDA. Springer; 2002. p. 189–208.
[34] Kapulla R, Najera SB. Operation conditions of a phase Doppler anemometer: droplet size measurements with laser beam power, photomultiplier voltage, signal gain and signal-to-noise ratio as parameters. Measur Sci Technol 2006;17(1):221–7.
[35] “DIN SPEC 91325:2015-06, Charakterisierung von Sprays und Sprühprozessen durch die Messung der Größe und der Geschwindigkeit nicht-transparenter Tropfen” 2015.
[36] Mulhem B, Schulte G, Fritsching U. Solid–liquid separation in suspension atomization. Chem Eng Sci 2006;61(8):2582–9.
[37] Hussein HJ, Capp SP, George WK. Velocity measurements in a high-Reynolds-number, momentum-conserving, axisymmetric, turbulent jet. J Fluid Mech 1994;258(–1):31.
[38] Lasheras JC, Villermaux E, Hopfinger EJ. Break-up and atomization of a round water jet by high-speed annular air jet. J. Fluid Mech. 1998;357:351–79.
[39] Varga CM, Lasheras JC, Hopfinger EJ. Initial breakup of a small-diameter liquid jet by a high-speed gas stream. J. Fluid Mech. 2003;497:405–34.